Analytical Treatment of EPR Spectra of Weakly Coupled Spin-Correlated Radical Pairs in Disordered Solids: Application to the Charge-Separated State in TiO_2 Nanoparticles

A. A. Dubinski and G. D. Perekhodtsev

Institute of Chemical Physics, Russian Academy of Sciences, Moscow 117977, Russia

O. G. Poluektov, T. Rajh, and M. C. Thurnauer*

Chemistry Division, Argonne National Laboratory, Argonne, Illinois 60439

Received: August 24, 2001

An analytical treatment of spin-correlated radical pair EPR spectra for the general case of weakly coupled spins is presented. In contrast to the multiparametric computer simulation of these spin-polarized EPR spectra, the analytical treatment reveals the relationship and rules that clarify the physical interpretation of the spectra. The analytical treatment developed here is applied to an analysis of the spin-polarization pattern of time-resolved EPR spectra of TiO_2 nanoparticles, recorded with the light-modulation technique. It is shown that the experimental spectra are satisfactorily fitted within the model of spin-correlated radical pairs for which the S_0 and T_0 or T_+ and T_- levels are initially populated. Only a weak dipole−dipole interaction is required for spectral fitting. Computer simulation of the spectra allows for a determination of the range of distances between the trapped electron within the TiO_2 particle and the trapped hole on the surface of the particle.

1. Introduction

Spin-correlated transient pairs of paramagnetic particles generated by photoinitiated charge separation have been studied in biologically relevant species[1−8] and artificial biomimetic systems.[9−12] Spectra of spin-correlated pairs detected by time-resolved EPR methods depend on numerous parameters that characterize the structure of the individual radicals, their spin−spin interactions, and the spin-level populations. The anisotropy of paired centers in disordered solids results in overlapping signals of differently oriented pairs and drastically complicates the spectra. Analysis of such spectra requires their computer simulation based on a complete set of parameters. Some of the parameters are a priori unknown and must be varied until the simulation fits the experimental spectrum. Thus, the goal of the analysis can be formally expressed as the elucidation of certain unknown fitting parameters. The procedure of multiparametric computer simulations of EPR spectra is well-characterized and can be fulfilled for any set of parameters. However, this total simulation procedure precludes a ready interpretation of the spectra.

Recently, we reported enhanced charge separation in nanocrystalline TiO_2 particles.[13] This process involves reversible photoinduced interfacial electron transfer from surface modifiers into the conduction band of the TiO_2 nanoparticles. By using time-resolved EPR spectroscopy, electron-spin-polarized spectra of the charge-separated state were recorded. To give a clear physical interpretation of the spin-polarization phenomena in the TiO_2 nanoparticles, we present here a detailed analytical treatment of the spin-correlated radical pair EPR spectra of weakly coupled spins. A brief description of this approach was previously presented in ref 14. Application of this treatment to nanocrystalline TiO_2 particles provides a satisfactory fit to the experimental time-resolved EPR spectra within the model of spin-correlated radical pairs. We demonstrate that only dipole−dipole interactions are required for a spectral fit. Computer simulation of the spectra allows for a determination of the range of distances between the trapped electron within the TiO_2 particle and the trapped hole on the surface of the particle, as well as an orientational selectivity in the electron transfer from the surface modifier to the trapping site in the nanoparticle. The proposed analytical treatment of the spectra reveals the relationships and rules that clarify the physical interpretation of the spectra and can be used in general cases of weakly coupled spins. (Note that, during the preparation of this manuscript for publication our attention was drawn to a recently published article by Y. Kondrashkin and A. van der Est, *Spectrochim. Acta A* **2001**, *57*, 1697−1709, where a similar approach was employed for the interpretation of the spin-polarized spectra of the charge-separated states in the bacterial reaction center protein.)

2. Differential Effect in Spectra of Weakly Interacting Pairs

We consider the pair of radicals A and B ($S_{A,B} = {}^1/_2$) separated by a distance large enough to make exchange and dipole spin−spin interactions small compared to the difference between the resonance frequencies of individual radicals, that is, $\omega_{SS} \ll |\omega_A - \omega_B|$. Under these conditions, the Hamiltonian can be truncated to the secular part

$$H = \omega_A \hat{S}_{Az} + \omega_B \hat{S}_{Bz} + \omega_{SS} \hat{S}_{Az} \hat{S}_{Bz} \qquad (1)$$

where ω_{SS} is the sum of the exchange and dipole−dipole interaction terms, that is, $\omega_{SS} = (J + D)$. The dipole splitting term, D, has the well-known dependence on the distance between the paired radicals, r_{AB}, and on the angle θ_{AB} between the pair director and external field

* Author to whom correspondence should be addressed.

10.1021/jp013276h CCC: $22.00
Published on Web 01/04/2002

$$D = (\beta^2 g_A g_B/\hbar r^3_{AB})(1 - 3\cos^2\theta_{AB}) \quad (2)$$

The energy level diagram of such a pair is shown at Figure 1. The transition frequencies of radicals A and B are shifted from their "isolated" positions ω_A and ω_B by $\pm\omega_{SS}/2$ because of a weak spin−spin interaction. This shift can be treated in terms of the pair interaction field, $H_{SS} = \pm(\hbar\omega_{SS})/(2g\beta)$, induced on the radical A by spin B (and vice versa) in addition to the external field H_0. The interaction field can be either positive or negative depending on the α or β state of the inducing spin. If the spin-level populations correspond to the high-temperature Boltzmann equilibrium, then the EPR lines that are related to transitions of radicals A and B, are split as shown at Figure 1b. The radical pair spectrum thus consists of the four lines

$$F_{AB}(H) = (Np_B/2)\{[f_A(H+H_{SS}) + f_A(H-H_{SS})] + [f_B(H+H_{SS}) + f_B(H-H_{SS})]\} \quad (3)$$

where f_A and f_B are normalized spectra of individual radicals A and B, respectively; N is the number of pairs; and $p_B = g\beta H/kT$ is a Boltzmann factor. The lines of radicals A and B can be considered independent from each other, and we analyze below only one of their contributions (e.g., A) omitting indices

$$[F(H)]_{eq} = (Np_B/2)[f(H+H_{SS}) + f(H-H_{SS})] \quad (4)$$

The interaction field splitting, $2H_{SS}$, if measured from experimental spectra, gives the spin−spin interaction frequency. However, when this splitting is smaller than the width of the spectral component $f(H)$, it is not resolved and contributes to a small broadening of the experimental line. This broadening can be evaluated with a deconvolution approach.[15] In the case of weak spin coupling, this approach is problematic because of the experimental noise and minor line shape distortions.

When these pairs are detected not in equilibrium but rather in a spin-polarized state, interesting possibilities arise for determining small spin−spin splittings. Such polarization can occur for spin-correlated radical pairs generated by light-induced charge separation. For instance, when the pair originates from an excited singlet state of an electron donor S*, conservation of zero spin projection at high magnetic fields requires than only the states $|\alpha\beta>$ and $|\beta\alpha>$ are populated, but not the $|\alpha\alpha>$ and $|\beta\beta>$ states. For this population distribution, the EPR transitions appear in counter phase [e.g., *A*(absorption)/*E*(emission); see Figure 1c], and their lines subtract instead of add as in eq 4

$$[F(H)]_{pol} = (N/2)[f(H+H_{SS}) - f(H-H_{SS})] \quad (5)$$

For a small splitting, the difference in eq 5 can be substituted by a differential

$$[F(H)]_{pol} = NH_{SS}\frac{d}{dH}f(H) \quad (6)$$

Thus, the splitting information is contained in the spectral amplitude and can be determined by comparison of amplitudes of the polarized spectrum and the reference equilibrium spectrum in its derivative form, $[F(H)]_{ref}$. The latter must be detected under the same experimental conditions, but after thermalization of the spin-level populations via spin−lattice relaxation

$$[F(H)]_{ref} = \frac{d}{dH}[F(H)]_{eq} = (Np_B)\frac{d}{dH}f(H) \quad (7)$$

It follows that direct amplitude measurement yields the values of the spin−spin coupling

$$H_{SS} = p_B[F(H)]_{pol}/[F(H)]_{ref} \quad (8)$$

The differential spectral line shape for polarized spin-correlated radical pairs (eq 6) was derived for the simplest case of pairs consisting of particles having homogeneous line widths $f_{A,B}(H)$. In cases where the lines are inhomogeneous, i.e., contain a multitude of resonances at different magnetic fields, H_{res}, the signal from each radical, $F(H)$, can be represented as a convolution

$$F(H) = \int_{-\infty}^{\infty} f(H-H_{res})\, q(H_{res})\, dH_{res} \quad (9)$$

where $q(H_{res})$ is a resonance field distribution function. For spin-polarized radical pairs, the pair interaction field splits each line into a counterphase doublet, which results in

$$[F(H)]_{pol} = N\frac{d}{dH}\int_{-\infty}^{\infty}[f(H-H_{res})\, q(H_{res})]H_{SS}\, dH_{res} \quad (10)$$

In disordered solids, which are the great majority of samples, spectra of pairs are summed over different orientations. In this case, H_{SS} is altered because of the anisotropy of the dipole−dipole interaction (see eq 2). If the local magnetic interactions of radicals are anisotropic, resonance fields of spin packages also depend on orientations [$H_{res} = H_{res}(\vartheta,\varphi)$], and the expression for the line shape of the polarized spin-correlated radical pairs can be written as

$$[F(H)]_{pol} = (N/4\pi)\frac{d}{dH}\int_{-\infty}^{\infty}[f(H-H')]\, dH' \int_0^{2\pi} d\varphi \int_0^{\pi}\delta[H' - H_{res}(\vartheta,\varphi)]\, H_{SS}[\theta_{AB}(\vartheta,\varphi,\eta,\phi)]\sin\vartheta\, d\vartheta \quad (11)$$

where ϑ and φ are the polar angles of the laboratory field axis in the molecular frame of the radical. The angle θ_{AB} between the direction of the magnetic field and the pair director depends on ϑ and φ, and as well as on the angles η and ϕ, which determine the director in the molecular frame as shown at Figure 2. Equation 11 allows for a simple and easily understood treatment of the spectral line shape.

3. Separation of Exchange and Dipole−Dipole Interactions

The pair interaction field H_{SS} is a sum of exchange and dipole contributions

$$H_{SS} = H_J + H_D$$

where $H_J = J/g\beta$, $H_D = H_{D\perp}(1 - 3\cos^2\theta_{AB})$, and $H_{D\perp} = (g\beta/\hbar r^3_{AB})$. Therefore, the spectrum $[F(H)]_{pol}$ derived in eq 11 consists of two additive parts, the exchange-polarized and dipole-polarized spectra

$$[F(H)]_{pol} = [F(H)]_{polJ} + [F(H)]_{polD} \quad (12)$$

The exchange-dependent contribution is

$$[F(H)]_{polJ} = NH_J\frac{d}{dH}\int_{-\infty}^{\infty}[f(H-H_{res})]\, q(H_{res})\, dH_{res} = NH_J\frac{d}{dH}F(H) \quad (13)$$

In the absence of the dipole−dipole contribution, the polarized pair spectrum in disordered samples has a derivative shape of the equilibrium spectrum, and its relative amplitude can be used

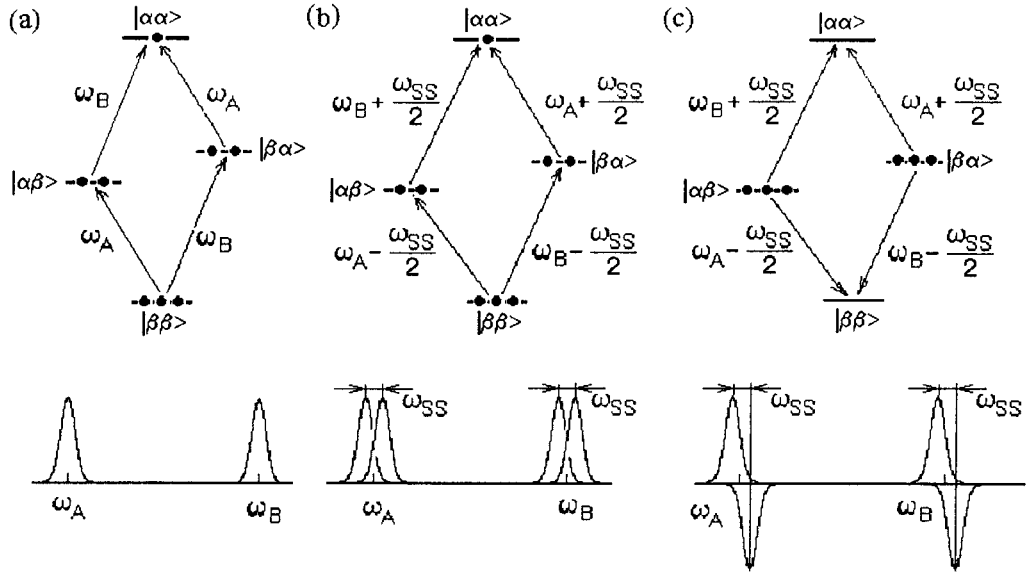

Figure 1. Diagrams of energy levels and their relative populations of radical pairs: (a) without spin−spin interaction, (b) with weak spin−spin interaction in Boltzmann equilibrium state, and (c) with weak spin−spin interaction in spin-polarized state. The respective spectra are shown schematically at the bottom.

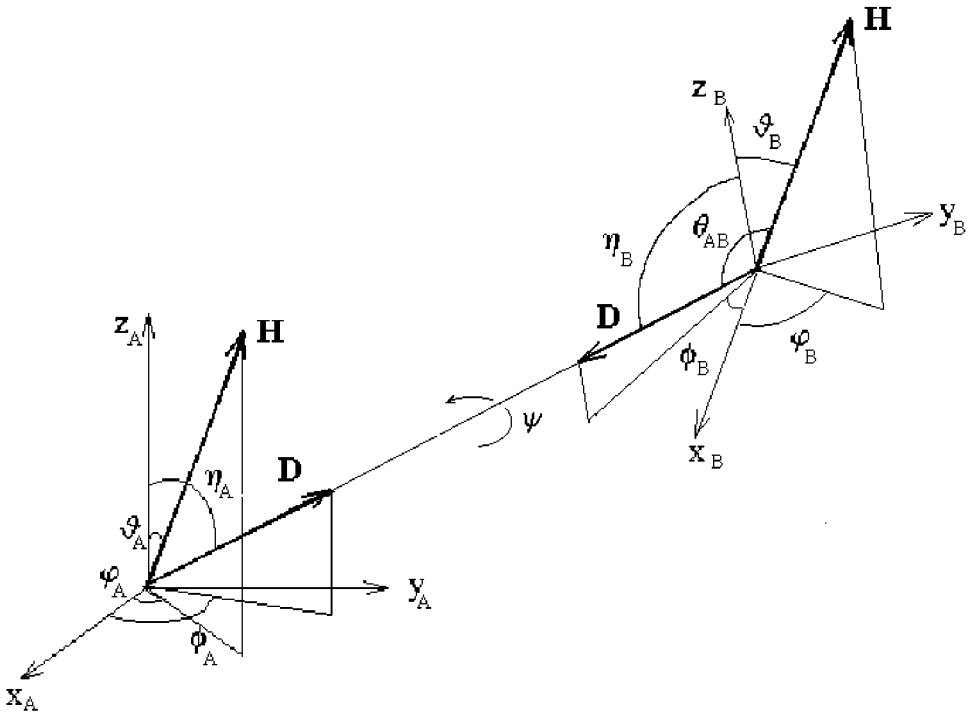

Figure 2. Definition of radical pair angles described in text. Radicals A and B are shown in their molecular frames.

to evaluate the exchange interaction according to eq 8. When the dipole contribution is present, it can be discriminated from the exchange contribution to allow for their separate analyses. Such discrimination can be fulfilled by the procedure outlined below.

According to eq 11, double integration of the experimental spectrum $[F(H)]_{pol}$ of the radical pair results in

$$I^{(2)}_{pol} = \int_{-\infty}^{\infty} dH \int_{-\infty}^{H} [F(H')]_{pol}\, dH' = N(H_J + H_{D\perp}<1 - 3\cos^2\theta_{AB}>) = NH_J \quad (14)$$

Averaging over the random distribution of radical pairs results in a total cancellation of the dipole contribution. The double integral of the reference spectrum, $[F(H)]_{ref}$, equals the single integral of the equilibrium spectrum, $[F(H)]_{eq}$ (see eq 7)

$$I^{(2)}_{ref} = \int_{-\infty}^{\infty} dH \int_{-\infty}^{H} [F(H')]_{ref}\, dH' = Np_B \quad (15)$$

Combining eqs 13−15 gives the spectral contribution of the exchange interaction as

$$[F(H)]_{polJ} = [F(H)]_{ref} I^{(2)}_{pol}/p_B \quad (16)$$

Therefore, the dipole spectral contribution can be obtained as

$$[F(H)]_{polD} = [F(H)]_{pol} - [F(H)]_{ref} I^{(2)}_{pol}/p_B \quad (17)$$

Note that this decomposition procedure is based only on the experimental spectra $[F(H)]_{pol}$ and $[F(H)]_{eq}$ and does not require

any spectral simulation. Also simulation of the shape of the pure exchange-polarized spectral contribution is not required. The shape is a derivative of the experimental equilibrium spectrum.

For weakly coupled pairs of radicals separated by a large distance, the exchange interaction occurs mostly by indirect pathways via "chains" of intermediate overlapping orbitals. Thus, the experimentally determined exchange interaction is an important characteristic associated with electron transfer along these chains and can be correlated, for instance, with the pair recombination rates.[16,17] However, the indirect exchange does not characterize the pair geometry. On the other hand, the dipole interaction is directly related to the pair structure.

4. Dipole Interaction Contribution

The dipole splitting H_D can be expressed as

$$H_{D\perp}(1 - 3\cos^2\theta_{AB}) = H_{D\perp}[1 - 3(h_x^2 d_x^2 + h_y^2 d_y^2 + h_z^2 d_z^2) + 6(h_x d_x h_y d_y + h_x d_x h_z d_z + h_z d_z h_y d_y)] \quad (18)$$

where h_i and d_i are direction cosines of the field and pair directors in the molecular frame, respectively. They are determined by $(h_x, h_y, h_z) = (\sin\vartheta\cos\varphi, \sin\vartheta\sin\varphi, \cos\vartheta)$ and $(d_x, d_y, d_z) = (\sin\eta\cos\phi, \sin\eta\sin\phi, \cos\eta)$ (for definitions see Figure 2). Substituting eq 18 into eq 11, one obtains

$$[F(H)]_{polD} = NH_{D\perp}\{(1 - 3d_x^2)F_{xx}(H) + (1 - 3d_y^2)F_{yy}(H) + (1 - 3d_z^2)F_{zz}(H) + 6[d_x d_y F_{xy}(H) + d_y d_z F_{yz}(H) + d_z d_x F_{zx}(H)]\} \quad (19)$$

where

$$F_{ij}(H) = (1/2\pi)\frac{d}{dH}\int_{-\infty}^{\infty}[f(H-H')]\,dH'\int_0^{2\pi}d\varphi\int_0^{\pi}\delta[H' - H_{res}(\vartheta,\varphi)]h_i h_j \sin\vartheta\,d\vartheta \quad (20)$$

Equation 19 shows that the dipole interaction contribution to the polarized spectrum consists of the six basic additive lines $F_{ij}(H)$. Their shapes are independent of the pair geometry and depend only on the characteristics of the paired radical contained in $H_{res}(\vartheta,\varphi)$, which can be determined from an analysis of the equilibrium spectrum of the individual radicals. Below, we assume that these characteristics are known a priori for the paired radicals. The pair geometry parameters, r_{AB}, η, and ϕ, contribute only to the coefficients of the partial lines, $F_{ij}(H)$, in eq 19. Actually, these three parameters are related to the spectrum of one of the paired radicals, say A, characterized by $H_{resA}(r_{AB},\eta_A,\phi_A)$. The spectral domain of radical B is also described by eqs 19 and 20 as $H_{resB}(r_{BA},\eta_B,\phi_B)$. Because the pair directors with respect to the frames of radicals A and B are different (see Figure 2), the angles η_A, ϕ_A and η_B, ϕ_B are independent, whereas $r_{AB} = r_{BA}$. Thus, the total number of independent pair geometry parameters is five. Note that one more angle exists that completes the full description of the pair geometry: ψ, the tilt angle of radicals about the pair director shown at Figure 2. However, this angle does not influence the dipole-polarized spectrum and cannot be determined from its analysis.

An important consequence of the decomposition in eq 19 is that the dipole interaction term $H_{D\perp}(r_{AB})$ determines only the absolute amplitudes of the spectral components and has no influence on the line shapes. The overall line shape of the spectrum is determined by the angular coefficients. Despite the large number of coefficients, six for A and six for B, they each depend only on two pairs of angles. Therefore, these angles can be evaluated from any two pairs of coefficients from the independent decomposition of the spectra of A and B according to eq 19.

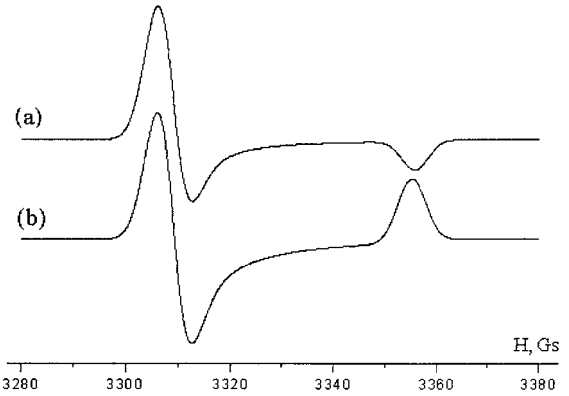

Figure 3. X-band EPR spectra simulation for one radical in a radical pair with axial g symmetry, $g_{xx} = g_{yy} = 1.98$, $g_{zz} = 1.95$: (a) equilibrium spectrum and (b) dipole-polarized spectrum.

The decomposition in eq 19 can be achieved if the lines $F_{ij}(H)$ can be easily distinguished from each other. The higher the symmetry of the local anisotropy function $H_{res}(\vartheta,\varphi)$, the fewer the parameters required in eq 20. Indeed, if the paired radicals are both isotropic and if H_{res} does not depend on orientation, then the powder average in eq 20 equals zero for all lines $F_{ij}(H)$. This results in the *complete vanishing* of the dipole-polarized spectrum. Note that this cancellation occurs in the presence of a dipole interaction as a result of the isotropic symmetry of the paired radicals. If one partner in the pair is anisotropic, it gives a nonzero dipole contribution to the spectrum.

In cases where a paired radical has axial symmetry, its dipole-polarized spectrum (eq 19) is reduced to a single line

$$[F(H)]_{polD} = NH_{D\perp}(1 - 3d_z^2)F_{axi}(H) \quad (21)$$

where

$$F_{axi}(H) = (1/4\pi)\frac{d}{dH}\int_{-\infty}^{\infty}[f(H-H')]\,dH'\int_0^{2\pi}d\varphi\int_0^{\pi}\delta[H' - H_{res}(\vartheta,\varphi)](1 - 3\cos^2\vartheta)\sin\vartheta\,d\vartheta \quad (22)$$

Equation 21 is similar to eq 13 for the exchange contribution. The line shape is the same for any magnitude of the dipole interaction. The explicit derivative shape of $F_{axi}(H)$ is modified by the angular term $(1 - 3\cos^2\vartheta)$ in eq 22. This term results in inversion and a 2-fold amplitude increase of the parallel canonical peak (where $\vartheta = 0$) with respect to the perpendicular one (where $\vartheta = 90°$), as shown in Figure 3. Thus, the amplitude ratios of the polarized and equilibrium spectra give the only experimental parameter that contains the pair geometry characteristics. These parameters combine distance and angular factors, $H_{D\perp}(r_{AB})$ and $(1 - 3\cos^2\eta)$, that cannot be discriminated. Such discrimination requires additional independent information.

In the case of $\eta = 54°$ ("magic angle"), $(1 - 3\cos^2\eta) = 0$, and the dipole spectrum vanishes. Note that, in this case, the line amplitude equals zero despite a finite dipole interaction for most orientations of the pair. The powder averaging results in total cancellation of the dipole spectrum as in the case of isotropic radicals described above.

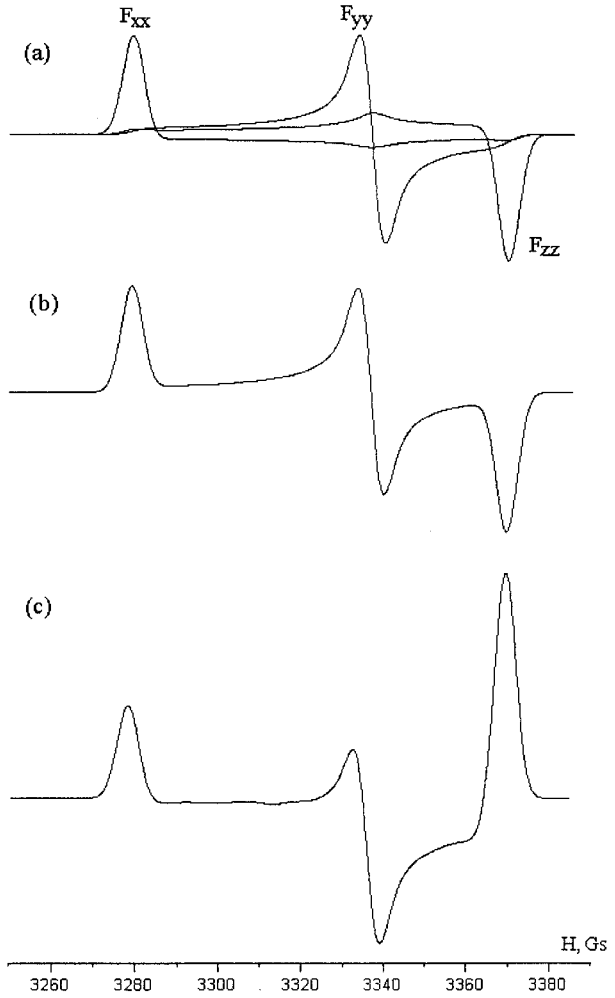

Figure 4. X-band EPR spectra simulation for one radical in a radical pair with rhombic g symmetry, $g_{xx} = 2.015$, $g_{yy} = 1.98$, $g_{zz} = 1.96$: (a) basic decomposition lines F_{ii}, (b) equilibrium spectrum, and (c) dipole-polarized spectrum with the dipole vector axis angle $\eta = 0$.

Further reduction of the local anisotropy of the paired radicals occurs if the angular dependence of the resonance field originates from a rhombic symmetry of the effective g values, $g_{\text{eff}} = (g_{xx}^2 h_x^2 + g_{yy}^2 h_y^2 + g_{zz}^2 h_z^2)^{1/2}$, or from that of the hyperfine constants, $A_{\text{eff}} = (A_{xx}^2 h_x^2 + A_{yy}^2 h_y^2 + A_{zz}^2 h_z^2)^{1/2}$. In these cases, H_{res} has mirror symmetry with respect to the molecular frame planes, and the powder averaging in eq 20 results in cancellation for $i \neq j$. Moreover, even when the local anisotropy of a radical originates from a combination of interactions (i.e., g, A) having differently oriented main axes, the last three terms in eq 19 and can be neglected. Thus, the dipole spectrum in the general case can be represented as

$$[F(H)]_{\text{pol}D} = NH_{\text{D}\perp}\{(1 - 3d_x^2)F_{xx}(H) + (1 - 3d_y^2)F_{yy}(H) + (1 - 3d_z^2)F_{zz}(H)\} \quad (23)$$

For the case of g anisotropy large enough to resolve canonical peaks in the spectrum of one of the paired radicals, lines F_{ii} are exemplified in Figure 4. Each line has an appreciable amplitude only at the respective canonical position. The sum of the basic lines results in the explicit derivative line shape

$$F_{xx}(H) + F_{yy}(H) + F_{zz}(H) = \frac{\mathrm{d}}{\mathrm{d}H}F(H) \quad (24)$$

Moreover, when the canonical peaks of the derivative spectrum are well-resolved, their shapes and amplitudes coincide exactly with those of the corresponding lines F_{ii} (see Figure 4). In the dipole spectrum (eq 23), these amplitudes are scaled by the angular coefficients $(1 - 3d_i^2)$, and the amplitudes can be used to evaluate these coefficients. If the angle between the dipole vector and the main magnetic axis of the radical is 54° (magic angle), the corresponding canonical peak vanishes. For well-resolved spectra, the amplitude ratios in the dipole and reference spectra give three factors, $\Delta H_{\text{D}i} = H_{\text{D}\perp}(1 - 3d_i^2)$, which are actually the dipole splittings for the ith canonic orientation of the paired radical. This evaluation does not require any spectral simulation. In the case of poorly resolved spectra, the dipole splittings can be found by fitting the dipole spectrum as a sum of lines F_{ii} simulated according to eq 20 with parameters of the individual radicals.

The three dipole splittings $\Delta H_{\text{D}i}$ are not independent because of the relationship

$$\Delta H_{\text{D}x} + \Delta H_{\text{D}y} + \Delta H_{\text{D}z} = 0 \quad (25)$$

As in the axial case above, the number of parameters available from the line shape analysis is less than the number of variables describing the pair geometry, and a complete description requires additional information. Even when the dipole splittings can be resolved and directly measured at the canonical peaks of the spectrum of paired radicals (also in the equilibrium spectrum), eq 25 does not allow for elucidation of the pair distance and orientation angles simultaneously. Only the absolute values of the dipole coupling can be obtained from the equilibrium spectrum. However, decomposition of the polarized spectra over the basic lines F_{ii} gives both their magnitudes and their signs. This is very useful in cases where both the dipole and exchange interactions are significant in the pair. Indeed, in these cases, canonical splittings are $\Delta H_i = \Delta H_{\text{D}i} + \Delta H_{\text{J}}$, and their algebraic sum determines the exchange interaction via

$$\Delta H_{\text{J}} = (\Delta H_x + \Delta H_y + \Delta H_z)/3 \quad (26)$$

This evaluation of the exchange splitting is more exact and reliable than the integration procedure outlined in the previous section and can also be used for separating the dipole and exchange parts of the polarized spectrum.

Even though the line shape analysis of the polarized spectra of weakly interacting pairs does not yield a complete set of geometric parameters, it provides certain structural information. If the dipole spectrum represented in eq 23 is recast as

$$[F(H)]_{\text{pol}D} = NH_{\text{D}\perp}(1 - 3d_z^2)[\chi F_{xx}(H) - (1 + \chi)F_{yy}(H) + F_{zz}(H)] \quad (27)$$

where

$$\chi = (1 - 3d_x^2)/(1 - 3d_z^2) \quad (28)$$

and $(1 - 3d_z^2) \neq 0$ is assumed, the partial contributions of the basic lines are determined only by the parameter χ, which can be easily evaluated. For instance, if the amplitudes of the resolved canonical peaks of the dipole spectrum are A_i and those of the equilibrium spectrum are A_i^0, one finds $\chi = A_i A_j^0 / A_i^0 A_j$. Equation 28 determines a range of orientations allowed for the dipole vector in the molecular frame as shown in Figure 5.

When the radical pairs do not have a single structure but rather exhibit a limited distribution of geometries, their polarized spectra can be represented by eqs 13 and 23 with $<H_{\text{J}}>$ and $<H_{\text{D}\perp}(1 - 3d_i^2)>$ averaged over the distribution. In the case

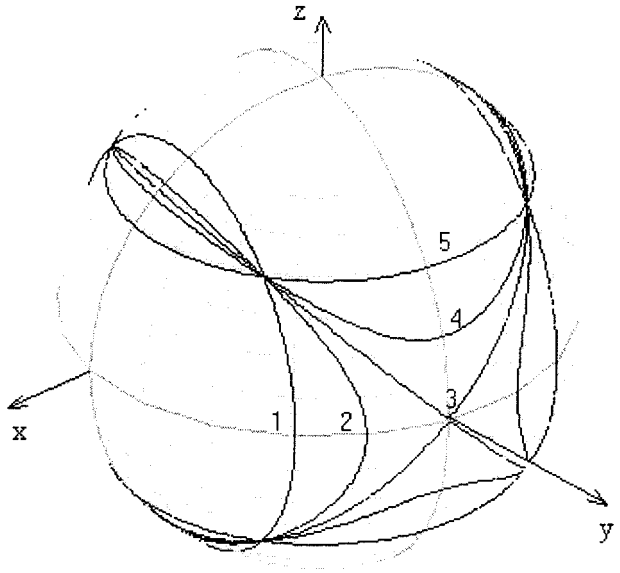

Figure 5. Orientations of the pair axes allowed at different values of χ. Sphere plotted lines correspond to (1) $\chi = 0.01$, (2) $\chi = 0.667$, (3) $\chi = 1.0$, (4) $\chi = 1.5$, and (5) $\chi = 100$.

where the paired radical has an arbitrary orientation with respect to the dipole vector, the dipole-polarized spectrum vanishes completely. Thus, the presence of the dipole-polarized spectrum established by inspection of the experimental spectrum indicates an orientation-ordered pair structure.

5. Analysis of the Spin-Polarized Spectrum in TiO_2 Nanoparticles

The approach described above can be applied to an analysis of recently observed spectra of transient spin-correlated radical pairs generated at low temperature by the photolysis of TiO_2 nanoparticles.[13] The surface of these ~45-Å particles is specially modified with ascorbic acid, which is an electron-donating bidentate ligand.[18] Illumination with visible light induces electron transfer from the surface modifier into the conduction band of the nanocrystalline TiO_2 particles. These systems have an important property that charge pairs are instantaneously separated into two phases, with the holes on the donating organic modifier and the electrons in the conduction band of TiO_2. Furthermore, the charge separation is reversible at low temperatures, and the spin-polarized spectrum can be obtained using transient EPR techniques.

For an analysis of the spin polarization, the individual equilibrium spectra of the hole stabilized on the ascorbic acid radical, $R^{\bullet+}$, and the trapped electron on TiO_2, $R^{\bullet-}$, were simulated with axial g tensors $g(R^{\bullet+}) = (2.004, 2.004, 2.000)$ and $g(R^{\bullet-}) = (1.988, 1.988, 1.958)$.[18] Best fits were obtained by assuming anisotropy of the line widths originating from unresolved hyperfine interactions: $\Delta H(R^{\bullet+}) = (4.3\text{ G}, 4.3\text{ G}, 5.6\text{ G})$ and $\Delta H(R^{\bullet-}) = (2.5\text{ G}, 2.5\text{ G}, 7.0\text{ G})$. This set of individual magnetic parameters was used to simulate the equilibrium, exchange derivative, and dipole derivative lines for both radicals according to eqs 9, 13, and 23. Because of the local axial symmetry, only one dipole line contributes to each radical spectrum (see eq 21). The best fit shown in Figure 6 was simulated without any contribution of the equilibrium spectrum and with the dipole contribution dominating over the exchange contribution: $H_{D\perp}\langle 1 - 3d_z^2\rangle/H_J \approx -15$. One important conclusion from our analysis is that the observation of the spin polarization assumes a nonvanishing angular average $\langle 1 - 3d_z^2\rangle$, i.e., electron transfer and trapping on TiO_2 occur with high orientational selectivity with respect to the radical stabilized on the ascorbic acid.

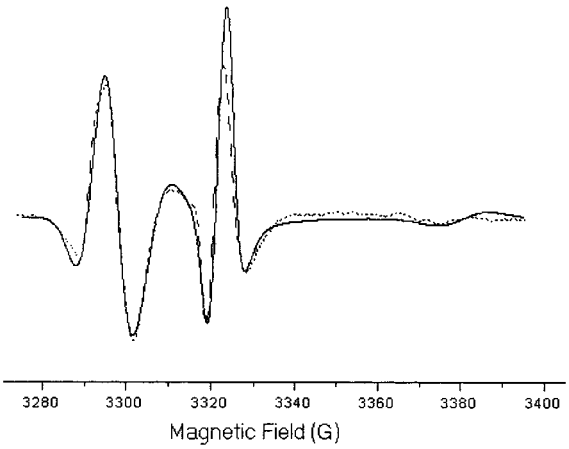

Figure 6. Simulated (solid line) and experimental (dotted line) spectra of radical pairs in nanocrystalline TiO_2 modified with ascorbic acid.

The transient spectra were observed using light/field modulation detection which results in the derivative line shape of the polarized spectrum (Figure 6). This mode of detection excludes the possibility of comparing amplitudes of the transient and equilibrium spectra and thus of determining the dipole coupling. However, our simulation shows that the experimental data can be fit only if the dipole−dipole interaction is less than 3.5 G. This corresponds to a distance between the unpaired electrons of greater than 20 Å (see eq 2), which, in combination with the size of nanoparticles (~45 Å), leads to the conclusion that the electron is localized near the center of the particle or on the particle side opposite the hole. This estimate is further supported by the reported ~15-Å separation for the exciton in TiO_2 nanoparticles.[19] Indeed, the interaction for the exciton is larger than that for the radical pair;[13] hence, the separation in the radical pair should be at least greater than 15 Å. Localization of the electron at the center or at the opposite side from the hole, stabilized on the modifier molecule, can also explain the orientational selectivity of the electron transfer and trapping. The axis of the magnetic interactions and the symmetry of the electron trapped on the interior Ti^{3+} ion should be determined by the D_{2d} symmetry of the anatase crystal structure. On the other hand, the symmetry of the trapped hole is determined by the structure that results from bidentate ligand binding, i.e., the symmetry of the surface modifier on which the hole is trapped. Thus, the relative orientations of the trapped electron and trapped hole magnetic tensors are fixed, leading to a nonvanishing angular average $\langle 1 - 3d_z^2\rangle$.

6. Conclusion

As shown above, the analytical treatment of EPR spectra of spin-polarized radical pairs in disordered solids is possible under the condition of weak spin−spin interactions within a radical pair. Such a spectrum is composed of simple and easily recognized spectral lines that are the derivative form of the equilibrium spectra of paired radicals and the basic decomposition spectra of the so-called "dipole contribution". These components are independent of the pair structure and are determined only by parameters of the individual pair-forming radicals. The pair structure defines partial contributions of these components and their intensities relative to the intensity of the equilibrium spectrum of the same pair. Elucidation of the pair geometry parameters from the polarized spectrum is reduced to finding the decomposition coefficients. This task becomes

especially simple for spectra with well-resolved canonical peaks in which all available combinations of the geometry coefficients can be determined as ratios of explicitly measured peak amplitudes. The basic restriction on this approach is that the parameters that can be obtained from the polarized spectra are underdetermined by one. This must be considered in pair structure studies where additional information is required for complete analysis of the pair geometry.

Acknowledgment. Work at ANL was supported by the U.S. Department of Energy, Office of Basic Energy Sciences, Division of Chemical Sciences, under Contract W-31-109-Eng-38. Work at the Institute of Chemical Physics RAS, Moscow, Russia, was supported by the Russian Foundation of Basic Researches (RFBR), No. 99-03-33252.

References and Notes

(1) Thurnauer, M. C.; Norris, J. *Chem. Phys. Lett.* **1980**, *76*, 557−561.

(2) Closs, G. L.; Forbes, M. D. E.; Norris, J. *J. Phys. Chem*. **1987**, *91*, 3592−3599.

(3) Buckley, C. D.; Hunter, D. A.; Hore, P. J.; MacLaughlan, K. A. *Chem. Phys. Lett.* **1987**, *135*, 307−312.

(4) Norris, J. R.; Morris, A. L.; Thurnauer, M. C.; Tang, J. *J. Chem. Phys.* **1990**, *92*, 4239−4249.

(5) Angerhofer, A.; Bittl, R. *Photobiology* **1996**, *63*, 11−38.

(6) Berthold, T.; Bechtold, M.; Heinen, U.; Link, G.; Poluektov, O.; Utschig, L.; Tang, J.; Thurnauer, M. C.; Kothe, G. *J. Phys. Chem. B* **1999**, *103*, 10733−10736.

(7) Snyder, S. W.; Thurnauer, M. C. In *The Photosynthetic Reaction Center*; Deisenhofer, M., Noris, J., Eds.; Academic Press: New York, 1993; Vol. II, pp 285−329.

(8) Prisner T. F.; van der Est, A.; Bittl, R.; Lubitz, W.; Stehlik, D.; Moebius, K. *Chem. Phys.* **1995**, *194*, 361−370.

(9) Kiefer, A. M.; Kast, S. M.; Wasielewski, M. R.; Laukenmann, K.; Kothe, G. *J. Am. Chem. Soc.* **1999**, *121*, 188−198.

(10) Tarasov, V. F.; Forbes, M. D. E. *Spectrochim. Acta A* **2000**, *56A*, 245−263.

(11) Molin, Y. N. *Spin Polarization and Magnetic Effects in Radical Reactions*; Elsevier: Amsterdam, 1984.

(12) Thurnauer, M. C.; Meisel, D. *J. Am. Chem. Soc.* **1983**, *105*, 3729−3731.

(13) Rajh, T.; Poluektov, O. G.; Dubinski, A. A.; Wiederrecht, G.; Thurnauer, M. C.; Trifunac, A. *Chem. Phys. Lett.* **2001**, *344*, 31.

(14) Poluektov, O. G.; Utschig, L. M.; Tang, J.; Dubinski, A. A.; Schlesselman, S.; Thurnauer, M. C. *J. Appl. Magn. Reson*., in press.

(15) Rabenstein, M. D.; Shin, Y.-K. *Proc. Natl. Acad. Sci. USA* **1995**, 92, 8239−8243.

(16) Graige, M. S.; Paddock, M. L.; Bruce, J. M.; Feher, G.; Okamura, M. Y. *J. Am. Chem. Soc.* **1996**, *118*, 9005−9016.

(17) Calvo, R.; Abresch, E. C.; Bittl, R.; Feher, G.; Hofbauer, W.; Isaacson, R. A.; Lubitz, W.; Okamura, M. Y.; Paddock, M. L. *J. Am. Chem. Soc.* **2000**, *122*, 7327−7341.

(18) Rajh, T.; Nedeljkovic, J. M.; Chen, L. X.; Poluektov, O.; Thurnauer, M. C. *J. Phys. Chem. B* **1999**, *103*, 3515−3519.

(19) Tang, H.; Prasad, K.; Sanjines, R.; Schmid, P. E.; Levy, F. *J. Appl. Phys*. **1994**, *75*, 2042.